Enhanced impacts of ENSO on the Southeast Asian summer monsoon under global warming and associated mechanisms

Geophysical Research Letters

RESEARCH LETTER
10.1029/2023GL106437

Enhanced Impacts of ENSO on the Southeast Asian Summer Monsoon Under Global Warming and Associated Mechanisms

Shuheng Lin[1], Buwen Dong[2], and Song Yang[1,3]

[1]School of Atmospheric Sciences, Sun Yat-sen University, Southern Marine Science and Engineering Guangdong Laboratory (Zhuhai), Zhuhai, China, [2]National Centre for Atmospheric Science, Department of Meteorology, University of Reading, Reading, UK, [3]Guangdong Province Key Laboratory for Climate Change and Natural Disaster Studies, Sun Yat-sen University, Zhuhai, China

Abstract Based on outputs of 28 coupled models from the Phase 6 of the Coupled Model Intercomparison Project (CMIP6), we show that the response of the Southeast Asian summer monsoon to the El Niño-Southern Oscillation (ENSO) during post-ENSO summer will likely strengthen in a warmer climate, which can be attributed to concurrently weakened sea-surface temperature anomalies (SSTAs) in the western equatorial Pacific (WEP). The weakened WEP SSTAs are primarily caused by enhanced latent heat damping due to increased surface wind speed anomalies, which are associated with the eastward shift of the El Niño-induced anomalous Walker circulation due to El Niño-like sea surface temperature change in the tropical Pacific under global warming. Besides, the climatological zonal ocean currents will slow down due to the weakening of climatological Walker circulation, which also acts to weaken the WEP SSTAs via reducing the advection of anomalous temperature by the mean current.

Plain Language Summary As an important component of the Asian monsoon system, the Southeast Asian summer monsoon (SEASM) is crucial for the livelihoods of billions of people in East Asia, and is closely connected to a climate phenomenon called El Niño-Southern Oscillation (ENSO). Understanding how the relationship between SEASM and ENSO will change in the future is important for enhancing our knowledge of climate change in East Asia. Outputs of 28 climate models from the Phase 6 of the Coupled Model Intercomparison Project show that ENSO will exert enhanced impacts on the SEASM in a warmer climate. The enhanced influences of ENSO on the monsoon will exacerbate the reduction of rainfall over the western North Pacific during the post-El Niño summer. We find that such projected changes are mainly caused by weakened warm sea surface temperature (SST) anomalies (SSTAs) in the western equatorial Pacific (WEP). Further analyses indicate that the change in WEP SSTAs can be linked to the El Niño-like change in climatological SSTs in the tropical Pacific. This study depicts detailed physical processes responsible for the projected changes in ENSO's impacts on the SEASM.

Key Points:

- The effects of the El Niño-Southern Oscillation on the Southeast Asian summer monsoon will strengthen under global warming
- The enhanced El Niño's impacts result from the weakened warm sea-surface temperature (SST) anomalies in the western equatorial Pacific (WEP)
- The weakened WEP SST anomalies are related to the eastward shift of anomalous Walker circulation and the slackened mean zonal ocean currents

Supporting Information:

Supporting Information may be found in the online version of this article.

Correspondence to:

S. Yang,
yangsong3@mail.sysu.edu.cn

Citation:

Lin, S., Dong, B., & Yang, S. (2024). Enhanced impacts of ENSO on the Southeast Asian summer monsoon under global warming and associated mechanisms. *Geophysical Research Letters*, *51*, e2023GL106437. https://doi.org/10.1029/2023GL106437

Received 21 SEP 2023
Accepted 5 JAN 2024

Author Contributions:

Conceptualization: Shuheng Lin, Buwen Dong, Song Yang
Methodology: Shuheng Lin
Supervision: Buwen Dong, Song Yang
Visualization: Shuheng Lin
Writing – original draft: Shuheng Lin
Writing – review & editing: Buwen Dong, Song Yang

1. Introduction

The Southeast Asian summer monsoon (SEASM), also referred to as the western North Pacific (WNP) monsoon, is an important component of the Asian monsoon system; it has received tremendous attention in the climate research community due to its considerable impacts on both social economy and climate of East Asia (e.g., Lau & Yang, 1997; Lee et al., 2011; Z. Li et al., 2016; M. Lu et al., 2021, 2023; Qian & Yang, 2000; Wang et al., 2001; S. Yang & Lau, 2006). The SEASM usually commences in mid-May and exists until October, with a main domain around 120°–160°E, 10°–22°N of the WNP region (Lau & Yang, 1997; T. Li & Wang, 2005; Wang & Fan, 1999; Wang & Lin, 2002).

The interannual variability of the SEASM is strongly associated with the El Niño-Southern Oscillation (ENSO). The monsoon tends to be weaker (stronger) than normal during post-El Niño (La Niña) summer (Chang et al., 2000; Chou et al., 2009; R. Huang & Wu, 1989) through ENSO-induced anomalous WNP circulation. The El Niño-induced cold sea-surface temperature (SST) anomalies (SSTAs) in the WNP can stimulate an anomalous WNP anticyclonic circulation (WNPAC) as an atmospheric Rossby wave response during El Niño mature winter, and maintain it during following spring and summer via local air-sea interactions (Wang et al., 2000). During post-El Niño summer, the SST warming in the tropical Indian Ocean (TIO) (S. Li et al., 2008; B. Wu et al., 2010; Xie et al., 2009; J. Yang et al., 2007) and tropical North Atlantic (TNA) (R. Lu & Dong, 2005; Rong

et al., 2010; Takaya et al., 2021) can also maintain the anomalous WNPAC by triggering a warm Kelvin wave that propagates eastward to the WNP. Some studies also emphasized that the ENSO decaying pace may modulate the ENSO-WNPAC relationship (Chen et al., 2016; W. Jiang et al., 2019; M. Wu et al., 2020). When El Niño rapidly decays and transitions to La Niña developing phase, the cold SSTAs in the central and eastern equatorial Pacific could strengthen the anomalous WNPAC by stimulating a Rossby wave to its west (Wang et al., 2013; Xiang et al., 2013). Additionally, the cold SSTAs with the concurrent TIO warming lead to an increased Indo-Pacific zonal gradient of SSTAs that can reinforce the anomalous WNPAC by favoring the TIO-induced warm Kelvin wave (Cao et al., 2013; Chen et al., 2012; He & Zhou, 2015; Terao & Kubota, 2005; Wang et al., 2017). This study will be focused on the SST zonal gradient mechanism.

Given the significant local impacts of the SEASM, it is crucial to understand how ENSO's influences on the SEASM will change in the future. The projected changes of El Niño-related anomalous WNPAC under global warming have been investigated based on models from the Coupled Model Intercomparison Project Phase 5 (CMIP5, Taylor et al., 2012), but they remain controversial. Some studies argued that the El Niño-related TIO warming would be amplified by global warming, thereby enhancing the anomalous WNPAC (Hu et al., 2014; Tao et al., 2015; Zheng et al., 2011). However, recent studies proposed that the anomalous WNPAC may be weakened due to weakened atmospheric circulation response to the ENSO under global warming (He et al., 2019; W. Jiang et al., 2018). It has been demonstrated that the CMIP5 models show low inter-model consensus in the projected changes of anomalous WNPAC during the post-El Niño summer (M. Wu et al., 2020).

Recently, the outputs from the new generation of the CMIP models, namely, the CMIP6 (Eyring et al., 2016) have been released. Improvements have been reported in many aspects, in comparison with previous generations, including the dynamic cores and parameterizations for physical processes (Eyring et al., 2019; D. Jiang et al., 2020; Xin et al., 2020). Using a large number of CMIP6 models, He et al. (2022) found that the El Niño-induced anomalous WNPAC is likely to be enhanced under global warming, which may be related to the increased zonal gradient of SSTAs between the TIO and western equatorial Pacific (WEP). However, it is still unclear what the detailed mechanisms for these projected changes are under global warming. On the other hand, the latest study by Lin et al. (2024) has shown that some of the CMIP6 models are not able to reproduce the observed ENSO-WNPAC relationship. The future projections based on these models might be contaminated by the model biases. In this study, we use 28 CMIP6 models that can reasonably simulate the responses of the SEASM to the ENSO to investigate the projected changes of ENSO's influences on the SEASM under global warming and to elucidate associated physical processes.

2. Data and Methods

2.1. Data

Monthly observational and reanalysis data sets are used to evaluate the model simulations, including (a) the monthly SST data from the Hadley Centre Sea Ice and Sea Surface Temperature (HadISST) version 1 (Rayner et al., 2003) (1871–Present), (b) the monthly precipitation data from the Global Precipitation Climatology Project (GPCP) version 2.2 (Adler et al., 2003) (1979–Present), and (c) the monthly wind field from the European Centre for Medium-range Weather Forecast version 5 reanalysis (ERA5, Hersbach et al., 2020) (1950–Present).

The monthly mean outputs of the first realization from the 40 CMIP6 models are used (Table S1 in Supporting Information S1). The historical experiment (HIS) during 1950–1999 is defined as the present climate, while the SSP5-8.5 experiment (SSP585) during 2050–2099 is considered as the future warmer climate. All model outputs are horizontally interpolated onto the same $2.5° \times 2.5°$ grid using a bilinear interpolation method. Anomaly fields are obtained by calculating their deviations from the climatological seasonal cycle after linear trends are removed. To focus on the ENSO-SEASM relationship on the interannual timescale, a 4–108-month bandpass filter is applied to each field in the data set using the sixth-order Butterworth filter (Park & Burrus, 1987).

To reduce the possible influence of model biases, we select 28 models with good performances in reproducing the observed ENSO's impacts on the SEASM to investigate future projections (Table S1 and Figure S1 in Supporting Information S1). Detailed descriptions of the selection of models can be seen in Text S1 in Supporting Information S1.

2.2. Regression Analysis

The averaged SSTAs in the Niño-3.4 region (170°–120°W, 5°S–5°N) during December–February (DJF) is used to depict ENSO variability. The SEASM index is defined as the horizontal shear of 850-hPa zonal wind between

(90°–130°E, 5°–15°N) and (110°–140°E, 22.5°–32.5°N) (Wang & Fan, 1999). A negative index value denotes an anomalous anticyclonic circulation in the region and thus indicates a weak SEASM, and vice versa. Following previous studies (W. Jiang et al., 2018; M. Wu et al., 2021), the anomaly fields are regressed onto the standardized Niño-3.4 index to obtain the ENSO-induced anomalies, which contain the influence of ENSO amplitude. The anomaly fields are also regressed onto the original Niño-3.4 index to represent the ENSO-induced anomalies without the effect of ENSO amplitude (non-amplitude factor; see Text S2 in Supporting Information S1 for detail). The standard two-tailed Student's t test is used to evaluate the significance levels of regressed anomalies. For the multi-model ensemble (MME) of projected changes in regressed anomalies, a threshold of 68% inter-model consensus is regarded as the 95% statistical significance according to previous studies (W. Jiang et al., 2018; Power et al., 2012). The change is considered significant if at least 19 of the 28 selected models agree on the sign of change.

2.3. Budget Analysis of Mixed-Layer Temperature

A heat budget analysis of mixed-layer temperature anomalies is used to explore the physical processes governing the evolution of WEP SSTAs in post-ENSO year, which is calculated as follows (Qu, 2003; Wang & Li, 1995):

$$\frac{\partial T'}{\partial t} = \underbrace{-u'\frac{\partial \overline{T}}{\partial x}}_{\mathrm{ZA}} \underbrace{-v'\frac{\partial \overline{T}}{\partial y}}_{\mathrm{VA}} \underbrace{-W_e'\left(\frac{\overline{T-T_e}}{h}\right)}_{\mathrm{EK}} \underbrace{-\overline{u}\frac{\partial T'}{\partial x}}_{\mathrm{MAU}} \underbrace{-\overline{v}\frac{\partial T'}{\partial y}}_{\mathrm{MAV}} \underbrace{-\overline{W_e}\left(\frac{(T-T_e)'}{h}\right)}_{\mathrm{TH}}$$
$$\underbrace{-\left(u'\frac{\partial T'}{\partial x}+v'\frac{\partial T'}{\partial y}+W_e'\frac{(T-T_e)'}{h}\right)}_{\mathrm{NDH}} + \underbrace{\frac{Q'_{\mathrm{net}}}{\rho_0 C_p h}}_{Q} + R, \quad (1)$$

where an overbar represents climatology and a prime denotes anomaly. T is ocean temperature averaged in the mixed layer and T_e is the temperature below it. U and V denote zonal and meridional horizontal current velocities averaged in the mixed layer, respectively. W_e represents vertical entrainment velocity, calculated as $W_e = (\partial h/\partial t) + (\partial hu/\partial x) + (\partial hv/\partial y)$. Q_{net} is the net surface heat flux (positive downward), including net shortwave (SW), longwave (LW), latent heat flux (LH), and sensible heat flux (SH). ρ_0 and C_p are density (1.029×10^3 kg m^{-3}) and specific heat capacity (3,996 J kg^{-1} K^{-1}) of sea water, respectively. h is the mixed-layer depth, which is defined based on meeting a "sigma-t (density)" criterion introduced by Levitus (1982), with a typical critical density difference of 0.03 kg m^{-3} in the CMIP6 models (Griffies et al., 2016). Detailed descriptions of terms on the right of Equation 1 can be found in Text S3 in Supporting Information S1.

3. Results

3.1. Projected Changes in ENSO's Impacts on SEASM

Figure 1a displays MME changes in ENSO-induced JJA(1) precipitation and 850-hPa wind anomalies for the period 2050–2099 relative to 1950–1999. A significant anticyclonic circulation change dominates over the WNP, accompanied by prominently decreased rainfall. These projected changes suggest strengthening SEASM's responses to the ENSO in a warmer climate. To further prove that the changes in ENSO-related SEASM anomalies are forced by global warming rather than by decadal internal variability, we show 50-year running regressions of JJA(1) SEASM index onto standardized D(0)JF(1) Niño-3.4 index in Figure 1b. The decadal variation of the ENSO-monsoon relationship is largely suppressed in the MME, and the externally forced signal is thus extracted. The MME shows an increasing trend since the early twentieth century, which becomes more significant as global warming intensifies. Besides, the signs of projected changes are agreed upon by more than 70% (20 out of the 28 models) of models (Figure S4a in Supporting Information S1). These results demonstrate the robustness of strengthened ENSO's impacts on the SEASM. Considering that the SEASM's responses to ENSO involve both ENSO amplitude and the non-amplitude factor (He et al., 2022; W. Jiang et al., 2018; M. Wu et al., 2021), we decompose the changes in ENSO-related SEASM anomalies into these two components (see Text S2 in Supporting Information S1 for detail). It is found that the changes in the non-amplitude factor dominate the changes in ENSO-related SEASM anomalies (Figure S4b in Supporting Information S1). Therefore, in the following analyses we focus on changes in ENSO-related variability without the effect of changes in ENSO amplitude.

10.1029/2023GL106437

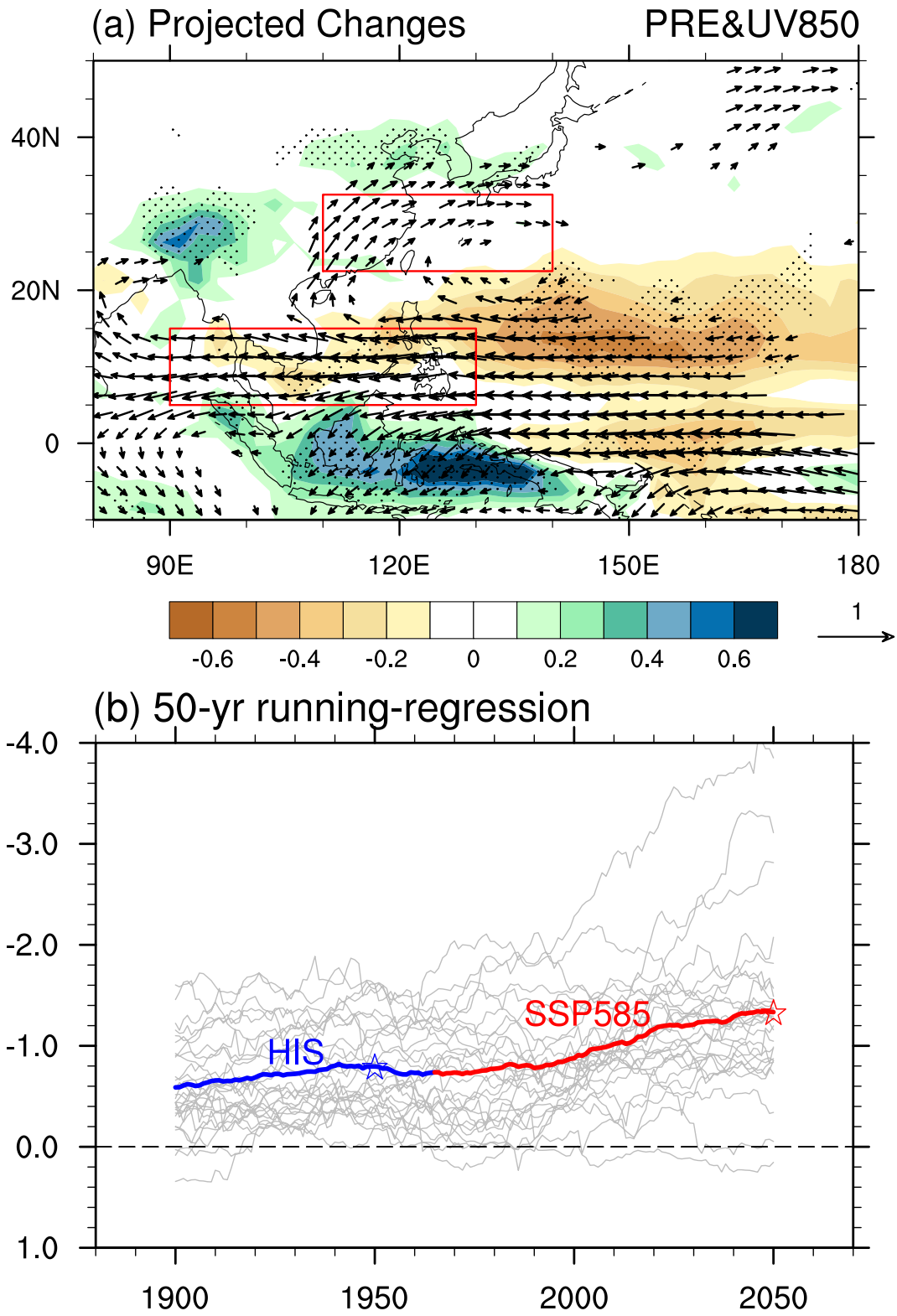

Figure 1.

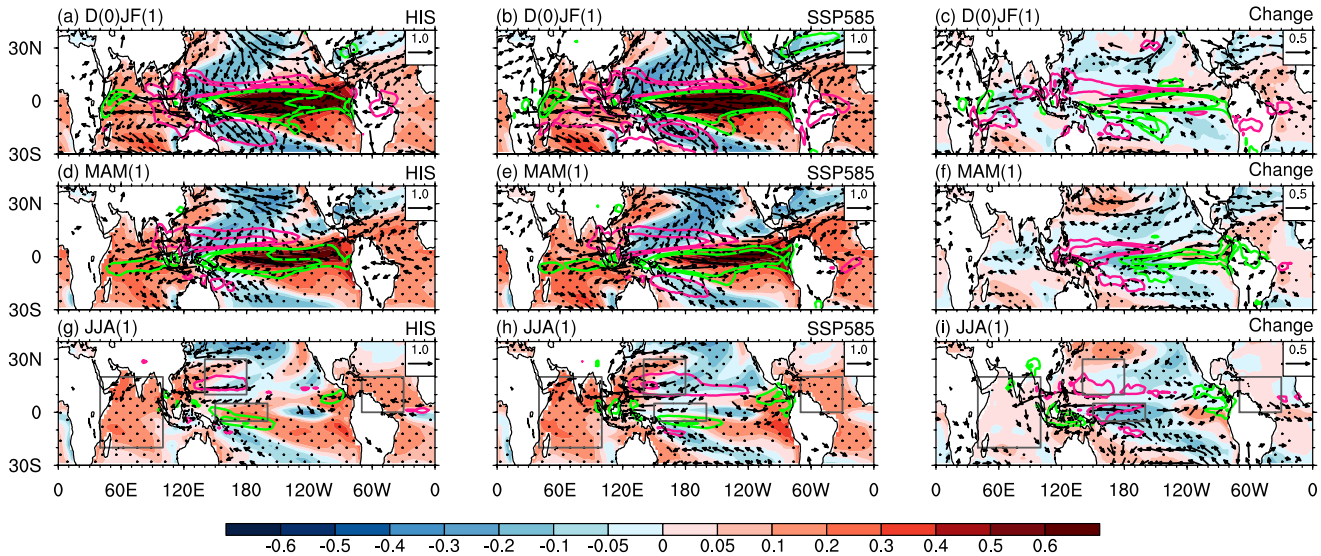

Figure 2. Regressed sea surface temperature (shading; units: °C), precipitation (contour; units: mm day^{-1}), and 850-hPa wind (vector; units: m s^{-1}) anomalies during El Niño mature winter [D(0)JF(1)] onto D(0)JF(1) Niño-3.4 index for (a) historical experiment (1950–1999), (b) SSP5-8.5 experiment (2050–2099), and (c) their differences. (d–f) Same as (a–c), but for post-El Niño-Southern Oscillation (ENSO) spring [MAM(1)]. (g–i) Same as (a, b), but for post-ENSO summer [JJA(1)]. In the left and middle panels, the green (red) lines represent the positive (negative) anomalies with 0.5 mm day^{-1} contour interval, and in the right panel they denote the positive (negative) change with 0.25 mm day^{-1} contour interval. Stippling in the left and middle panels represents significant, regressed anomalies at the 95% confidence level, while in the right panel it denotes the sign of multi-model ensemble-projected changes agreed by more than 68% of the models. Only the significant wind vectors above the 95% confidence level are plotted. The gray boxes in (g–i) indicate the western equatorial Pacific (WEP; 150°E–160°W, 5°S–5°N), western North Pacific (WNP; 40°–180°E, 10°–30°N), tropical Indian Ocean (TIO; 40°–100°E, 20°S–20°N), and tropical North Atlantic (TNA; 70°–30°W, 0°–20°N).

3.2. Physical Mechanisms for Changes in the Effect of ENSO on SEASM

Figure 2 shows spatial patterns in El Niño-related SST, 850-hPa wind, and precipitation anomalies for the historical experiments, SSP5-8.5 experiments, and their differences. The changes in TIO SST warming during post-El Niño summer are small, with a low model consensus (Figure 2i), which is different from the finding in He et al. (2022) that showed a significantly enhanced TIO warming based on the 40 CMIP6 models analyzed, implying that the projection of ENSO-induced TIO warming may be model dependent to some extent. Consistent with the insignificant change in TIO warming, the tropospheric temperature anomalies over TIO also show insignificant changes, indicating an insignificant change in the warm Kelvin wave excited by TIO warming (Figure S5g in Supporting Information S1). However, there exist significantly colder SSTAs in the WEP under the warmer climate, leading to an amplified zonal gradient of SSTAs between the TIO and WEP (Figures 2g–2i). The increased SST gradient intensifies the surface easterly wind anomalies over the maritime continent and WEP by enhancing the sea level pressure gradient (Lindzen & Nigam, 1987) (Figure S5h in Supporting Information S1). The enhanced equatorial wind anomalies can reinforce the anticyclonic wind shear and associated convection-circulation feedback over the WNP (Xie et al., 2009), thereby strengthening the anomalous WNPAC. Additionally, the negative change in SSTAs can cause reduced convection over the WEP, intensifying the WNPAC by stimulating a cold Rossby wave on its northwest (Figure 2i and Figure S5i in Supporting Information S1). In the TNA and WNP, the changes in SSTAs are also insignificant and small compared to those in the WEP during post-ENSO summer (Figure 2i and Figures S6b–S6d in Supporting Information S1). Furthermore, the projected changes in SEASM anomalies exhibit a strongly positive inter-model correlation (0.73; above 99% confidence level) with that in WEP SSTAs, while showing small and insignificant correlations with the WNP, TIO, and TNA SSTAs (Figure S7 in Supporting Information S1). Therefore, the enhanced El Niño's impacts on the SEASM under global warming are mainly related to the weakened warm SSTAs in the WEP during post-El Niño summer.

Figure 1. (a) Projected changes in regressed JJA(1) precipitation (shading; units: mm day^{-1}) and 850-hPa wind (vector; units: m s^{-1}) anomalies onto the standardized D(0)JF(1) Niño-3.4 index based on the multi-model ensemble (MME) of 28 selected CMIP6 models. Stippling indicates that the sign of MME-projected changes agreed by more than 68% of the models. (b) Fifty-year running-regression coefficients of JJA(1) Southeast Asian summer monsoon index onto the standardized D(0)JF(1) Niño-3.4 index. Labels on the *x*-axis denote the first year of a 50-year running window. Gray thin lines denote the results of individual models, and the thick lines denote the MME. The periods for historical and SSP5-8.5 experiments are indicated by blue and red lines, respectively. Here, the sliding windows covering the period after 2014 are classified as the SSP585 period. The blue and red stars highlight the periods of 1950–1999 and 2050–2099, respectively.

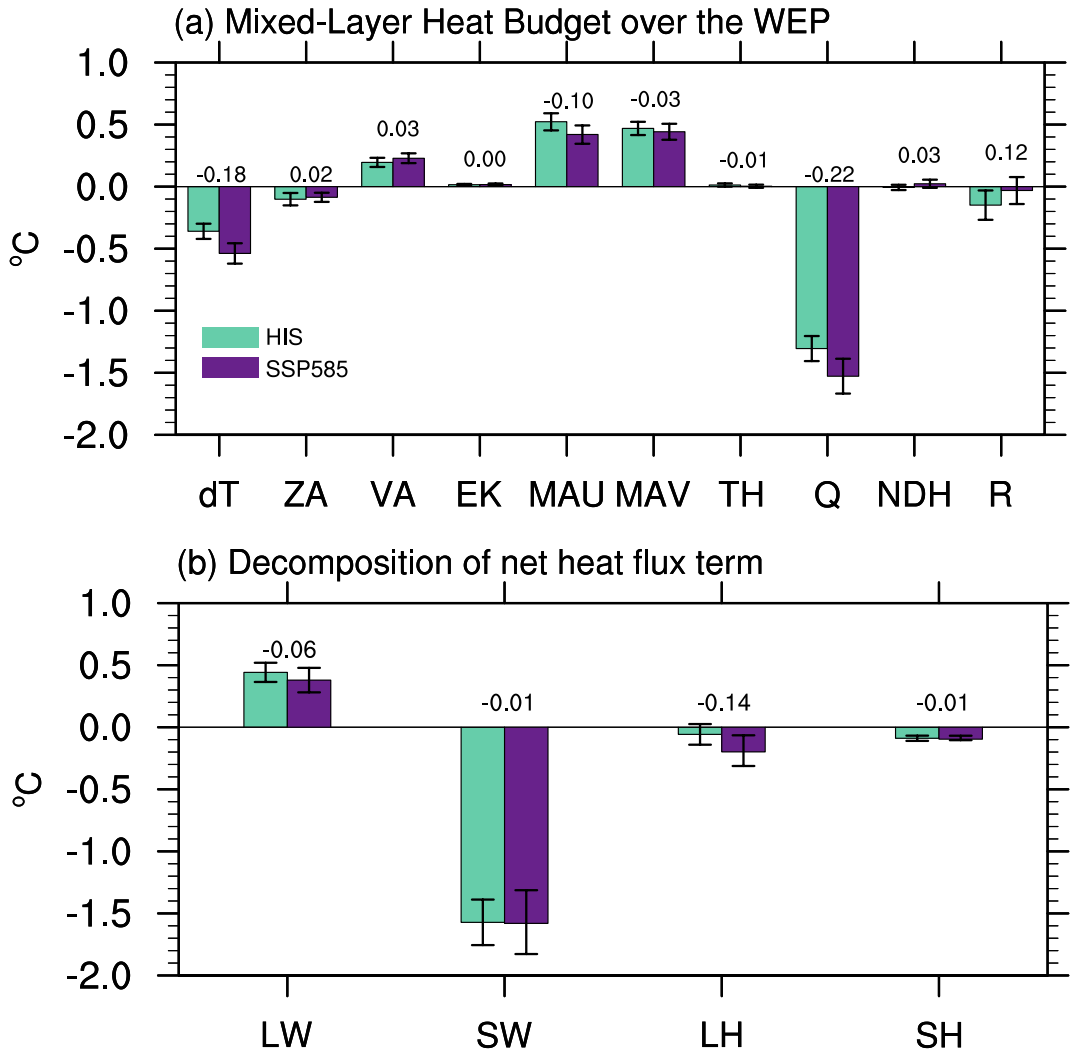

Figure 3. (a) Time-accumulated regressed mixed-layer heat budget terms from January(1) to June(1) averaged within western equatorial Pacific (150°E–160°W, 5°S–5°N) onto D(0)JF(1) Niño-3.4 index. (b) Decomposition of net heat flux term (Q). Green and purple bars denote the results of historical and SSP5-8.5 experiments, respectively. The error bars represent the 95% confidence intervals. The numbers show differences between the historical and SSP5-8.5 experiments.

The time evolutions of WEP SSTAs reveal a notably higher decaying rate of SSTAs from January(1) to June(1) but a comparable rate during JJA(1) in SSP585 compared to HIS (Figure S6a in Supporting Information S1). This result indicates that the formation of weakened WEP SSTAs during post-El Niño summer is attributed to the faster decay of the SSTAs from January(1) to June(1) (Figure S6a in Supporting Information S1). Therefore, we conduct a mixed-layer heat budget analysis from January(1) to June(1) to understand the change in SSTA evolution. The faster decay of mixed-layer temperature (DT, −0.18°C) in the future is primarily contributed by enhanced damping effect from the net heat flux term (Q, −0.22°C), while the decrease in anomalous warm zonal advection induced by mean zonal current (MAU $= -\overline{u}\frac{\partial T'}{\partial x}$, −0.1°C) plays a secondary role (Figure 3a). Furthermore, the change in LH anomaly (−0.14°C) dominates the change in Q anomaly (Figure 3b). The LH anomaly can be decomposed to the terms involving anomalous surface wind speed, specific humidity gradient between the ocean surface and surface air, and nonlinear process (see Figures S8a and S8b and Text S4 in Supporting Information S1). The decreases in surface wind speed term determine the enhanced negative LH anomalies from January to May (Figure S8c in Supporting Information S1). Moreover, the changes of LH in surface wind speed term mainly result from enhanced wind speed anomalies (Figure S8d in Supporting Information S1).

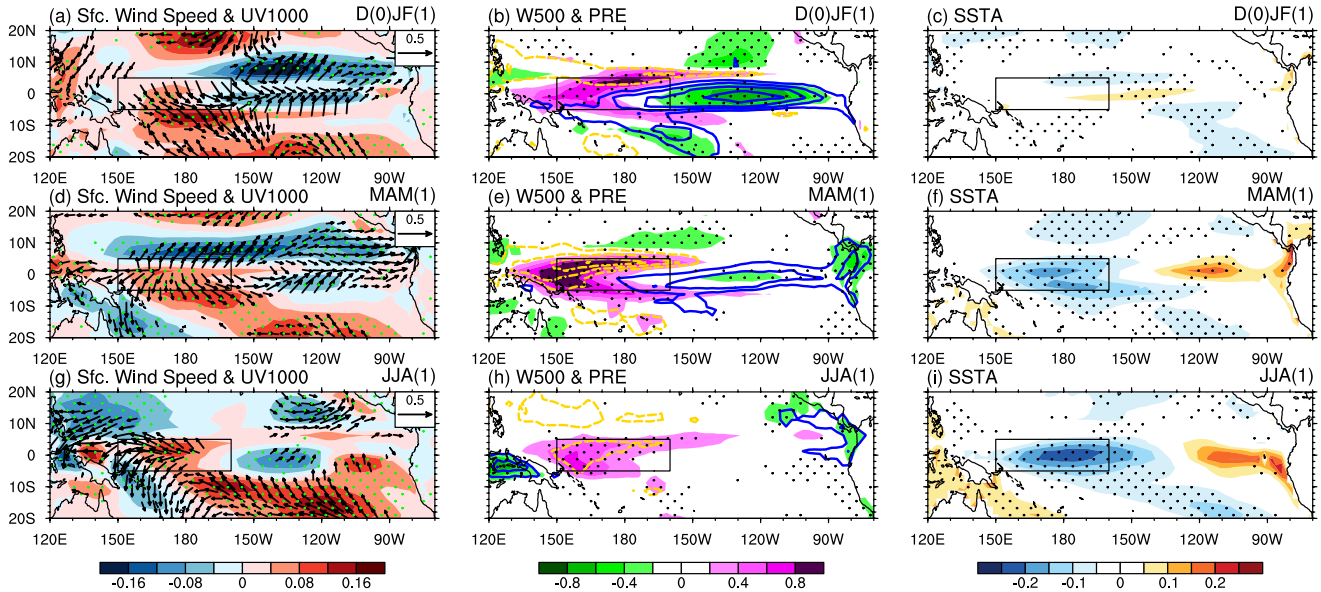

Figure 4. Projected changes in regressed surface wind speed (shading; units: m s^{-1}) and 1,000-hPa wind (vector; units: m s^{-1}) anomalies during (a) El Niño mature winter [D(0)JF(1)], (d) post-El Niño spring [MAM(1)], and (g) summer [JJA(1)] onto D(0)JF(1) Niño-3.4 index. (b, e, and h) Are the same as (a, d, and g), respectively, but for 500-hPa vertical velocity (shading; units: 10^{-2} Pa s^{-1}) and precipitation (contour; units: mm day^{-1}). Blue (yellow) contours denote positive and negative changes in precipitation anomaly with 0.3 mm day^{-1} contour interval. (c, f, and i) Are the same as (a, d, and g), respectively, but for sea-surface temperature anomalies. Stippling denotes the sign of multi-model ensemble-projected changes agreed by more than 68% of the models. Only significant wind vectors above the 95% confidence level (more than 68% model consensus) are plotted. The black boxes indicate the western equatorial Pacific.

Next, we investigate the process for the change in surface wind speed anomalies over the WEP. During El Niño mature winter, the spatial pattern of changes in surface wind anomalies over the western-central Pacific is characterized by divergence off the equator (along 5°N) and convergence at the equator (Figure 4a). The northerly wind anomalies thus prevail over the WEP, which can accelerate surface wind speed since there are climatological northerly winds over this region during the boreal winter and spring (Figure S9 in Supporting Information S1). These changes in surface wind anomalies are associated with the changes in the spatial structure of El Niño-induced anomalous Walker circulation (Figure 4b). The anomalous upward motions strengthen over the central-eastern Pacific, but weaken over the western Pacific, corresponding to a see-saw change in precipitation anomalies (Figure 4b). Such eastward shift of anomalous Walker circulation dominates the spatial change in El Niño-driven rainfall anomalies (Figures S10a–S10c in Supporting Information S1), as noted previously (P. Huang & Xie, 2015; Yan et al., 2020). Additionally, the increased rainfall over the central-eastern Pacific can favor the suppressed deep convection over the off-equatorial western Pacific (around 5°N) through stimulating northerly wind anomalies as Rossby wave responses on its west side to transport low climatological moist enthalpy from the subtropics, namely, the anomalous wind-moist enthalpy advection mechanism (B. Wu et al., 2017; Yan et al., 2020). Therefore, the maximum changes in vertical motion and precipitation anomaly are located at around 5°N over the WEP, corresponding to the center of surface divergence changes.

The changes in anomalous Walker circulation are primarily related to the changes in background SSTs in the tropical Pacific (P. Huang & Xie, 2015; P. Huang et al., 2017). The sensitivity of atmospheric deep convection response to SSTAs depends on the background SST with a nonlinear relationship between them due to the existence of SST threshold for convection (Graham & Barnett, 1987; Lau et al., 1997; Lin et al., 2022), which is approximately equal to the tropical-mean SST (Johnson & Xie, 2010; Vecchi & Soden, 2007a). The sensitivity is enhanced over the central-eastern equatorial Pacific with a relatively larger background SST warming than the tropical mean and weakened over the region with relatively smaller warming (Figures S11c and S11f in Supporting Information S1). The El Niño-like response of Pacific SSTs to global warming has been reported previously (e.g., Cai et al., 2015; Collins et al., 2010). Therefore, despite small changes in SSTAs in the equatorial Pacific (Figure 4c), the anomalous upward motion strengthens over the central-eastern equatorial Pacific but weakens over the WEP (Figure 4b). In post-El Niño spring, the formed WEP SST cooling further amplifies the decreased rainfall and suppressed deep convection over this region (Figures 4e and 4f). The surface divergence

winds thus develop over this region (Figure 4d), favoring the SST cooling tendency by enhancing surface evaporation (Figure S8c in Supporting Information S1). Consequently, the negative differences in SSTAs in the WEP associated with El Niño between the future and present climates become large and significant in post-El Niño summer (Figure 4i).

We also explore the reason for the changes in anomalous zonal advection induced by mean zonal current (MAU, Figure 3a). The decomposition of changes in MAU term demonstrates that the weakened mean zonal current in the mixed layer determines the decrease in MAU term (Figure S12a in Supporting Information S1), which is related to the slackened easterly trade wind over the equatorial Pacific (Figure S12b in Supporting Information S1). The weakening of climatological Walker circulation under global warming has been proposed by some researchers (Power & Smith, 2007; Tokinaga et al., 2012; Vecchi & Soden, 2007b), which is consistent with El Niño-like changes in the background SST (Figure S11f in Supporting Information S1). The significantly negative inter-model correlation further demonstrates the linkage between the changes in climatological SST and WEP SSTAs during post-El Niño summer (Figure S13 in Supporting Information S1).

4. Conclusions

Based on 28 CMIP6 models with good performances in representing the response of the SEASM to the ENSO, we investigate changes in ENSO's impacts on the SEASM during post-ENSO summer under global warming, with a focus on understanding associated mechanisms. We find that ENSO's influences on the SEASM will strengthen in a warmer climate, which can be attributed to the changes in ENSO-related WEP SSTAs. The warm SSTAs in the WEP during post-El Niño summer are projected to weaken due to the increased decaying rate of the SSTAs during El Niño mature winter and subsequent spring. Consequently, the enhanced SST gradient between the TIO and WEP favors a strengthening WNPAC. Mixed-layer heat budget analysis suggests that the fast decay of WEP SSTAs in a warmer climate primarily results from enhanced latent heat damping. Further analyses indicate that the changes in anomalous latent heat flux are determined by increased surface wind speed anomaly over the WEP, which is associated with the eastward shift of anomalous Walker circulation due to the El Niño-like change in the background SST under global warming. Such spatial structure change in ENSO-related circulation leads to enhanced surface divergence of wind anomalies over the WEP, thereby accelerating the climatological wind speed. On the other hand, the weakening of climatological Walker circulation results in slacked westward zonal ocean current, thereby causing the decrease in anomalous zonal advection related to mean zonal current, which also favors the fast decay of WEP SSTAs. The main processes are summarized in Figure S14 in Supporting Information S1.

Previous studies suggested that the intensity of anomalous WNPAC during post-El Niño summer can also be affected by the El Niño decaying pace (Chen et al., 2012, 2016; W. Jiang et al., 2019; M. Wu et al., 2020). The El Niño events with a short decaying phase can lead to a strong WNPAC, and vice versa. Nevertheless, there is an insignificant change in the ENSO decaying pace under global warming based on the CMIP6 model projections (Figure S15 in Supporting Information S1). How the different types of ENSO in terms of their decaying rates will change, and how this change will affect their relationship with the SEASM need further investigation.

Conflict of Interest

The authors declare no conflicts of interest relevant to this study.

Data Availability Statement

The HadISST data set is downloaded from the UK Met Office (https://www.metoffice.gov.uk/hadobs/hadisst/). The GPCP monthly precipitation data is provided by the NOAA PSL, Boulder, Colorado, USA, via the website (https://psl.noaa.gov/data/gridded/data.gpcp.html). The ERA5 monthly reanalysis data can be downloaded from Hersbach et al. (2023). The CMIP6 models used in this study are listed in Table S1 in Supporting Information S1, and their outputs are available at the Earth System Grid Federation (https://esgf-node.llnl.gov/search/cmip6/). All the data analysis and plotting are conducted with the software: NCAR Command Language

(NCL) version 6.6.2. The download and installation instructions of NCL can be found on the website (https://www.ncl.ucar.edu/Download/). The NCL codes of this study are available from the corresponding author upon request.

Acknowledgments
Authors thank the two anonymous reviewers for their constructive comments and suggestions on the early version of this paper and are grateful to all data providers. This research was supported by the National Natural Science Foundation of China (Grant 42088101), the Guangdong Major Project of Basic and Applied Basic Research (Grant 2020B0301030004), the Guangdong Province Key Laboratory for Climate Change and Natural Disaster Studies (Grant 2020B1212060025), the Innovation Group Project of Southern Marine Science and Engineering Guangdong Laboratory (Zhuhai) (Grant 311021001), and the China Scholarship Council Joint Ph.D. Training Program.

References

Adler, R. F., Huffman, G. J., Chang, A., Ferraro, R., Xie, P.-P., Janowiak, J., et al. (2003). The version-2 global precipitation climatology project (GPCP) monthly precipitation analysis (1979–Present). *Journal of Hydrometeorology*, *4*(6), 1147–1167. https://doi.org/10.1175/1525-7541(2003)004<1147:TVGPCP>2.0.CO;2

Cai, W., Santoso, A., Wang, G., Yeh, S. W., An, S. I., Cobb, K. M., et al. (2015). ENSO and greenhouse warming. *Nature Climate Change*, *5*(9), 849–859. https://doi.org/10.1038/nclimate2743

Cao, J., Lu, R., Hu, J., & Wang, H. (2013). Spring Indian Ocean-western Pacific SST contrast and the East Asian summer rainfall anomaly. *Advances in Atmospheric Sciences*, *30*(6), 1560–1568. https://doi.org/10.1007/S00376-013-2298-6/METRICS

Chang, C. P., Zhang, Y., & Li, T. (2000). Interannual and interdecadal variations of the East Asian summer monsoon and tropical Pacific SSTs. Part I: Roles of the subtropical ridge. *Journal of Climate*, *13*(24), 4326–4340. https://doi.org/10.1175/1520-0442(2000)013<4326:IAIVOT>2.0.CO;2

Chen, W., Lee, J. Y., Ha, K. J., Yun, K. S., & Lu, R. (2016). Intensification of the western North Pacific anticyclone response to the short decaying El Niño event due to greenhouse warming. *Journal of Climate*, *29*(10), 3607–3627. https://doi.org/10.1175/JCLI-D-15-0195.1

Chen, W., Park, J.-K., Dong, B., Lu, R., Jung, W.-S., Chen, W., et al. (2012). The relationship between El Niño and the western North Pacific summer climate in a coupled GCM: Role of the transition of El Niño decaying phases. *Journal of Geophysical Research*, *117*(D12), 12111. https://doi.org/10.1029/2011JD017385

Chou, C., Huang, L. F., Tu, J. Y., Tseng, L., & Hsueh, Y. C. (2009). El Niño impacts on precipitation in the western North Pacific–East Asian sector. *Journal of Climate*, *22*(8), 2039–2057. https://doi.org/10.1175/2008JCLI2649.1

Collins, M., An, S.-I., Cai, W., Ganachaud, A., Guilyardi, E., Jin, F.-F., et al. (2010). The impact of global warming on the tropical Pacific Ocean and El Niño. *Nature Geoscience*, *3*(6), 391–397. https://doi.org/10.1038/ngeo868

Eyring, V., Bony, S., Meehl, G. A., Senior, C. A., Stevens, B., Stouffer, R. J., et al. (2016). Overview of the coupled model intercomparison project phase 6 (CMIP6) experimental design and organization (pp. 1937–1958). https://doi.org/10.5194/gmd-9-1937-2016

Eyring, V., Cox, P. M., Flato, G. M., Gleckler, P. J., Abramowitz, G., Caldwell, P., et al. (2019). Taking climate model evaluation to the next level. *Nature Climate Change*, *9*(2), 102–110. https://doi.org/10.1038/s41558-018-0355-y

Graham, N. E., & Barnett, T. P. (1987). Sea surface temperature, surface wind divergence, and convection over tropical oceans. *Science*, *238*(4827), 657–659. https://doi.org/10.1126/science.238.4827.657

Griffies, S. M., Danabasoglu, G., Durack, P. J., Adcroft, A. J., Balaji, V., Böning, C. W., et al. (2016). OMIP contribution to CMIP6: Experimental and diagnostic protocol for the physical component of the Ocean Model Intercomparison Project. *Geoscientific Model Development*, *9*(9), 3231–3296. https://doi.org/10.5194/GMD-9-3231-2016

He, C., Cui, Z., & Wang, C. (2022). Response of western North Pacific anomalous anticyclones in the summer of decaying El Niño to global warming: Diverse projections based on CMIP6 and CMIP5 models. *Journal of Climate*, *35*(1), 359–372. https://doi.org/10.1175/JCLI-D-21-0352.1

He, C., & Zhou, T. (2015). Responses of the western North Pacific subtropical high to global warming under RCP4.5 and RCP8.5 scenarios projected by 33 CMIP5 Models: The dominance of tropical Indian Ocean–tropical western Pacific SST gradient. *Journal of Climate*, *28*(1), 365–380. https://doi.org/10.1175/JCLI-D-13-00494.1

He, C., Zhou, T., & Li, T. (2019). Weakened anomalous western North Pacific anticyclone during an El Niño-decaying summer under a warmer climate: Dominant role of the weakened impact of the tropical Indian Ocean on the atmosphere. *Journal of Climate*, *32*(1), 213–230. https://doi.org/10.1175/JCLI-D-18-0033.1

Hersbach, H., Bell, B., Berrisford, P., Biavati, G., Horányi, A., Muñoz Sabater, J., et al. (2023). ERA5 hourly data on pressure levels from 1940 to present [Dataset]. Copernicus Climate Change Service (C3S) Climate Data Store (CDS). https://doi.org/10.24381/cds.bd0915c6

Hersbach, H., Bell, B., Berrisford, P., Hirahara, S., Horányi, A., Muñoz-Sabater, J., et al. (2020). The ERA5 global reanalysis. *Quarterly Journal of the Royal Meteorological Society*, *146*(730), 1999–2049. https://doi.org/10.1002/QJ.3803

Hu, K., Huang, G., Zheng, X. T., Xie, S. P., Qu, X., Du, Y., & Liu, L. (2014). Interdecadal variations in ENSO influences on Northwest Pacific-East Asian early summertime climate simulated in CMIP5 models. *Journal of Climate*, *27*(15), 5982–5998. https://doi.org/10.1175/JCLI-D-13-00268.1

Huang, P., Chen, D., & Ying, J. (2017). Weakening of the tropical atmospheric circulation response to local sea surface temperature anomalies under global warming. *Journal of Climate*, *30*(20), 8149–8158. https://doi.org/10.1175/JCLI-D-17-0171.1

Huang, P., & Xie, S. (2015). Mechanisms of change in ENSO-induced tropical Pacific rainfall variability in a warming climate. *Nature Geoscience*, *8*(October), 922–927. https://doi.org/10.1038/NGEO2571

Huang, R., & Wu, Y. (1989). The influence of ENSO on the summer climate change in China and its mechanism. *Advances in Atmospheric Sciences*, *6*(1), 21–32. https://doi.org/10.1007/BF02656915

Jiang, D., Hu, D., Tian, Z., & Lang, X. (2020). Differences between CMIP6 and CMIP5 models in simulating climate over China and the East Asian monsoon. *Advances in Atmospheric Sciences*, *37*(10), 1102–1118. https://doi.org/10.1007/S00376-020-2034-Y/METRICS

Jiang, W., Huang, G., Huang, P., & Hu, K. (2018). Weakening of Northwest Pacific anticyclone anomalies during post-El Niño summers under global warming. *Journal of Climate*, *31*(9), 3539–3555. https://doi.org/10.1175/JCLI-D-17-0613.1

Jiang, W., Huang, G., Huang, P., Wu, R., Hu, K., & Chen, W. (2019). Northwest Pacific anticyclonic anomalies during post-El Niño summers determined by the pace of El Niño decay. *Journal of Climate*, *32*(12), 3487–3503. https://doi.org/10.1175/JCLI-D-18-0793.1

Johnson, N. C., & Xie, S. P. (2010). Changes in the sea surface temperature threshold for tropical convection. *Nature Geoscience*, *3*(12), 842–845. https://doi.org/10.1038/ngeo1008

Lau, K.-M., Wu, H. T., & Bony, S. (1997). The role of large-scale atmospheric circulation in the relationship between tropical convection and sea surface temperature. *Journal of Climate*, *10*(3), 381–392. https://doi.org/10.1175/1520-0442(1997)010<0381:TROLSA>2.0.CO;2

Lau, K.-M., & Yang, S. (1997). Climatology and interannual variability of the Southeast Asian summer monsoon. *Advances in Atmospheric Sciences*, *14*(2), 141–162. https://doi.org/10.1007/s00376-997-0016-y

Lee, S. S., Lee, J. Y., Ha, K. J., Wang, B., & Schemm, J. K. E. (2011). Deficiencies and possibilities for long-lead coupled climate prediction of the western North Pacific-East Asian summer monsoon. *Climate Dynamics*, *36*(5–6), 1173–1188. https://doi.org/10.1007/S00382-010-0832-0

Levitus, S. (1982). *Climatological atlas of the world ocean*. Professional Paper 13 (p. 173). NOAA/ERLGFDL. (NTISPB83-184093).

Li, S., Lu, J., Huang, G., & Hu, K. (2008). Tropical Indian Ocean basin warming and East Asian summer monsoon: A multiple AGCM study. *Journal of Climate*, *21*(22), 6080–6088. https://doi.org/10.1175/2008JCLI2433.1
Li, T., & Wang, B. (2005). A review on the western North Pacific monsoon: Synoptic-to-interannual variabilities. *Terrestrial, Atmospheric and Oceanic Sciences*, *16*(2), 285–314. https://doi.org/10.3319/TAO.2005.16.2.285(A
Li, Z., Yang, S., He, B., & Hu, C. (2016). Intensified springtime deep convection over the South China Sea and the Philippine Sea dries southern China. *Scientific Reports*, *6*, 1–9. https://doi.org/10.1038/srep30470
Lin, S., Dong, B., Yang, S., He, S., & Hu, Y. (2024). Causes of diverse impacts of ENSO on the Southeast Asian summer monsoon among CMIP6 models. *Journal of Climate*, *37*(2), 419–438. https://doi.org/10.1175/JCLI-D-23-0303.1
Lin, S., Yang, S., He, S., Li, Z., Chen, J., Dong, W., & Wu, J. (2022). Attribution of the seasonality of atmospheric heating changes over the western tropical Pacific with a focus on the spring season. *Climate Dynamics*, *58*(9), 2575–2592. https://doi.org/10.1007/s00382-021-06020-3
Lindzen, R., & Nigam, S. (1987). On the role of sea surface temperature gradients in forcing low-level winds and convergence in the tropics. *Journal of the Atmospheric Sciences*, *44*(17), 2418–2436. https://doi.org/10.1175/1520-0469(1987)044<2418:OTROSS>2.0.CO;2
Lu, M., Yang, S., Wang, J., Wu, Y., & Jia, X. (2021). Response of regional Asian summer monsoons to the effect of reduced surface albedo in different Tibetan Plateau domains in idealized model experiments. *Journal of Climate*, *34*(17), 7023–7036. https://doi.org/10.1175/JCLI-D-20-0500.1
Lu, M., Yang, S., Zhu, C., Wang, J., Lin, S., Wei, W., & Fan, H. (2023). Thermal impact of the southern Tibetan Plateau on the Southeast Asian summer monsoon and modulation by the tropical Atlantic SST. *Journal of Climate*, *36*(5), 1319–1330. https://doi.org/10.1175/JCLI-D-22-0493.1
Lu, R., & Dong, B. (2005). Impact of Atlantic sea surface temperature anomalies on the summer climate in the western North Pacific during 1997–1998. *Journal of Geophysical Research*, *110*(D16), 1–11. https://doi.org/10.1029/2004JD005676
Park, T. W., & Burrus, C. S. (1987). *Digital filter design*. John Wiley & Sons.
Power, S. B., Delage, F., Colman, R., & Moise, A. (2012). Consensus on twenty-first-century rainfall projections in climate models more widespread than previously thought. *Journal of Climate*, *25*(11), 3792–3809. https://doi.org/10.1175/JCLI-D-11-00354.1
Power, S. B., & Smith, I. N. (2007). Weakening of the Walker circulation and apparent dominance of El Niño both reach record levels, but has ENSO really changed? *Geophysical Research Letters*, *34*(18), 2–5. https://doi.org/10.1029/2007GL030854
Qian, W., & Yang, S. (2000). Onset of the regional monsoon over Southeast Asia. *Meteorology and Atmospheric Physics*, *75*(1–2), 29–38. https://doi.org/10.1007/s007030070013
Qu, T. (2003). Mixed layer heat balance in the western North Pacific. *Journal of Geophysical Research*, *108*(7), 1–13. https://doi.org/10.1029/2002jc001536
Rayner, N. A., Parker, D. E., Horton, E. B., Folland, C. K., Alexander, L. V., Rowell, D. P., et al. (2003). Global analyses of sea surface temperature, sea ice, and night marine air temperature since the late nineteenth century. *Journal of Geophysical Research*, *108*(14), 4407. https://doi.org/10.1029/2002jd002670
Rong, X. Y., Zhang, R. H., & Li, T. (2010). Impacts of Atlantic sea surface temperature anomalies on Indo-East Asian summer monsoon-ENSO relationship. *Chinese Science Bulletin*, *55*(22), 2458–2468. https://doi.org/10.1007/s11434-010-3098-3
Takaya, Y., Saito, N., Ishikawa, I., & Maeda, S. (2021). Two tropical routes for the remote influence of the northern tropical Atlantic on the Indo-western Pacific summer climate. *Journal of Climate*, *34*(5), 1619–1634. https://doi.org/10.1175/JCLI-D-20-0503.1
Tao, W., Huang, G., Hu, K., Qu, X., Wen, G., & Gong, H. (2015). Interdecadal modulation of ENSO teleconnections to the Indian Ocean basin mode and their relationship under global warming in CMIP5 models. *International Journal of Climatology*, *35*(3), 391–407. https://doi.org/10.1002/joc.3987
Taylor, K. E., Stouffer, R. J., & Meehl, G. A. (2012). An overview of CMIP5 and the experiment design. *Bulletin of the American Meteorological Society*, *93*(4), 485–498. https://doi.org/10.1175/BAMS-D-11-00094.1
Terao, T., & Kubota, T. (2005). East-west SST contrast over the tropical oceans and the post El Niño western North Pacific summer monsoon. *Geophysical Research Letters*, *32*(15), L15706. https://doi.org/10.1029/2005GL023010
Tokinaga, H., Xie, S.-P., Deser, C., Kosaka, Y., & Okumura, Y. M. (2012). Slowdown of the Walker circulation driven by tropical Indo-Pacific warming. *Nature*, *491*(7424), 439–443. https://doi.org/10.1038/nature11576
Vecchi, G. A., & Soden, B. J. (2007a). Effect of remote sea surface temperature change on tropical cyclone potential intensity. *Nature*, *450*(7172), 1066–1070. https://doi.org/10.1038/nature06423
Vecchi, G. A., & Soden, B. J. (2007b). Global warming and the weakening of the tropical circulation. *Journal of Climate*, *20*(17), 4316–4340. https://doi.org/10.1175/JCLI4258.1
Wang, B., & Fan, Z. (1999). Choice of South Asian summer monsoon indices. *Bulletin of the American Meteorological Society*, *80*(4), 629–638. https://doi.org/10.1175/1520-0477(1999)080<0629:COSASM>2.0.CO;2
Wang, B., Li, J., & He, Q. (2017). Variable and robust East Asian monsoon rainfall response to El Niño over the past 60 years (1957–2016). *Advances in Atmospheric Sciences*, *34*(10), 1235–1248. https://doi.org/10.1007/s00376-017-7016-3
Wang, B., Li, T., & Chang, P. (1995). An intermediate model of the tropical Pacific Ocean. *Journal of Physical Oceanography*, *25*(7), 1599–1616. https://doi.org/10.1175/1520-0485(1995)025<1599:AIMOTT>2.0.CO;2
Wang, B., & Lin, H. (2002). Rainy season of the Asian-Pacific summer monsoon. *Journal of Climate*, *15*(4), 386–398. https://doi.org/10.1175/1520-0442(2002)015<0386:RSOTAP>2.0.CO;2
Wang, B., Wu, R., & Fu, X. (2000). Pacific–East Asian teleconnection: How does ENSO affect East Asian climate? *Journal of Climate*, *13*(9), 1517–1536. https://doi.org/10.1175/1520-0442(2000)013<1517:PEATHD>2.0.CO;2
Wang, B., Wu, R., & Lau, K.-M. (2001). Interannual variability of the Asian summer monsoon: Contrasts between the Indian and the western North Pacific-East Asian monsoons. *Journal of Climate*, *14*(20), 4073–4090. https://doi.org/10.1175/1520-0442(2001)014<4073:IVOTAS>2.0.CO;2
Wang, B., Xiang, B., & Lee, J. Y. (2013). Subtropical high predictability establishes a promising way for monsoon and tropical storm predictions. *Proceedings of the National Academy of Sciences of the United States of America*, *110*(8), 2718–2722. https://doi.org/10.1073/PNAS.1214626110/SUPPL_FILE/PNAS.201214626SI.PDF
Wu, B., Li, T., & Zhou, T. (2010). Relative contributions of the Indian Ocean and local SST anomalies to the maintenance of the western North Pacific anomalous anticyclone during the El Niño decaying summer. *Journal of Climate*, *23*(11), 2974–2986. https://doi.org/10.1175/2010JCLI3300.1
Wu, B., Zhou, T., & Li, T. (2017). Atmospheric dynamic and thermodynamic processes driving the western North Pacific anomalous anticyclone during El Niño. Part I: Maintenance Mechanisms. *Journal of Climate*, *30*(23), 9621–9635. https://doi.org/10.1175/JCLI-D-16-0489.1
Wu, M., Zhou, T., & Chen, X. (2021). The source of uncertainty in projecting the anomalous western North Pacific anticyclone during El Niño–decaying summers. *Journal of Climate*, *34*(16), 6603–6617. https://doi.org/10.1175/JCLI-D-20-0904.1

Wu, M., Zhou, T., Chen, X., & Wu, B. (2020). Intermodel uncertainty in the projection of the anomalous western North Pacific anticyclone associated with El Niño under global warming. *Geophysical Research Letters*, *47*(2), e2019GL086139. https://doi.org/10.1029/2019GL086139

Xiang, B., Wang, B., Yu, W., & Xu, S. (2013). How can anomalous western North Pacific subtropical high intensify in late summer? *Geophysical Research Letters*, *40*(10), 2349–2354. https://doi.org/10.1002/GRL.50431

Xie, S. P., Hu, K., Hafner, J., Tokinaga, H., Du, Y., Huang, G., & Sampe, T. (2009). Indian Ocean capacitor effect on Indo-western Pacific climate during the summer following El Niño. *Journal of Climate*, *22*(3), 730–747. https://doi.org/10.1175/2008JCLI2544.1

Xin, X., Wu, T., Zhang, J., Yao, J., & Fang, Y. (2020). Comparison of CMIP6 and CMIP5 simulations of precipitation in China and the East Asian summer monsoon. *International Journal of Climatology*, *40*(15), 6423–6440. https://doi.org/10.1002/JOC.6590

Yan, Z., Wu, B., Li, T., Collins, M., Clark, R., Zhou, T., et al. (2020). Eastward shift and extension of ENSO-induced tropical precipitation anomalies under global warming. *Science Advances*, *6*(2), 1–11. https://doi.org/10.1126/sciadv.aax4177

Yang, J., Liu, Q., Xie, S. P., Liu, Z., & Wu, L. (2007). Impact of the Indian Ocean SST basin mode on the Asian summer monsoon. *Geophysical Research Letters*, *34*(2), 1–5. https://doi.org/10.1029/2006GL028571

Yang, S., & Lau, W. K.-M. (2006). Interannual variability of the Asian monsoon. In *The Asian monsoon* (pp. 259–293). Springer. https://doi.org/10.1007/3-540-37722-0_6

Zheng, X. T., Xie, S. P., & Liu, Q. (2011). Response of the Indian Ocean basin mode and its capacitor effect to global warming. *Journal of Climate*, *24*(23), 6146–6164. https://doi.org/10.1175/2011JCLI4169.1

References From the Supporting Information

Hayes, S. P., Chang, P., & McPhaden, M. J. (1991). Variability of the sea surface temperature in the eastern equatorial Pacific during 1986–1988. *Journal of Geophysical Research*, *96*(C6), 10553–10566. https://doi.org/10.1029/91JC00942

Jiang, W., Huang, G., Hu, K., Wu, R., Gong, H., Chen, X., & Tao, W. (2017). Diverse relationship between ENSO and the Northwest Pacific summer climate among CMIP5 models: Dependence on the ENSO decay pace. *Journal of Climate*, *30*(1), 109–127. https://doi.org/10.1175/JCLI-D-16-0365.1

Song, F., & Zhou, T. (2015). The crucial role of internal variability in modulating the decadal variation of the East Asian summer monsoon-ENSO relationship during the twentieth century. *Journal of Climate*, *28*(18), 7093–7107. https://doi.org/10.1175/JCLI-D-14-00783.1